Audio Engineering Society

Convention Paper 10623

Presented at the 153rd Convention
2022 October

Spider Design Optimization At The Buckling Limit

Andri Bezzola[1]

[1] *Samsung Research America*

Correspondence should be addressed to Andri Bezzola (andri.b@samsung.com)

ABSTRACT

Size and design constraints in products such as soundbars and TVs require loudspeaker spiders of small diameter to allow for large voice-coil excursion. Spider designs that undergo exceedingly large displacements can exhibit buckling of the spider rolls, resulting in very audible distortion. Such buckling events are non-trivial to simulate with finite element methods and often lead to solver non-convergence. When wrapping numerical optimization algorithms around the finite-element simulations to achieve optimal spider designs, it is important to ensure that all simulated designs can be solved without errors or convergence issues. The optimal spider design might be right within the buckling limits and an automated numerical optimization algorithm will need to be able to resolve some designs that exhibit buckling. This work shows how an augmented FEM method can be used to circumvent issues when employing numerical optimization for a spider design near its buckling limits.

1 Introduction

Smaller and thinner designs for TV audio modules set aggressive excursion limits on conventional transducers. For example, the 6-inch transducer in the subwoofer of the Samsung HW S800B soundbar has been designed to have excursion limits exceeding ± 25 mm. Such size requirements pose design challenges for all parts of the transducer. This work focuses on the specific design challenges for the spider. The spider's main task is to keep the voice coil, former, and diaphragm assembly centered to avoid rocking motion of the diaphragm or rubbing of the voice coil or former against the elements of the magnetic circuit. A secondary task of the spider is to aid the surround in creating a restoring force to keep the moving elements of the transducer centered in axial direction with the voice coil optimally located in the magnetic gap. In order to keep a high acoustic efficiency, the restoring force cannot be too high. The spider and surround must thus allow for large excursions of the voice coil without creating and unreasonably high restoring force. This restoring force is generally a nonlinear function function of voice-coil

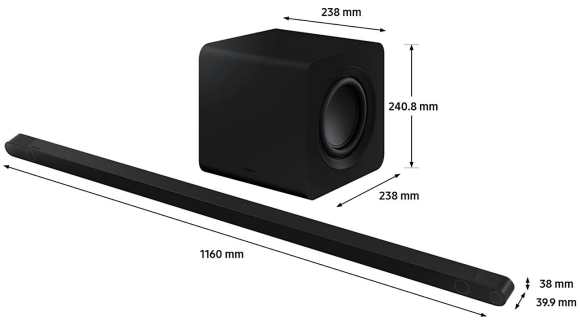

Fig. 1: The Samsung HW S800B soundbar and dimensions. Its subwoofer consists of an 8-liter enclosure with a 6-inch transducer and 8-inch passive radiator.

excursion.

For impregnated cloth spiders the major design parameters are number of rolls, height of rolls, and shape of roll tips [1]. The design variables are typically chosen to increase the linearity of the suspension, i.e., to keep the restoring force $F(x_{vc})$ a linear function of voice coil excursion x_{vc}. At maximum excursion, spiders are typically designed to progressively increase the stiffness, which provides a mechanical protection against the voice coil bottoming out inside the gap. This progressive nature of $F(x_{vc})$ can be relaxed in modern loudspeaker systems that employ control technologies to provide an electronic protection against bottoming out [2, 3].

Spider design increasingly relies on Finite Element Method (FEM) modeling to predict the linear and nonlinear behavior of $F(x)$ [4, 5, 6]. The use of modeling methods also allow the application of numerical design optimization to tune a transducer design to a defined target [7, 8, 9, 10]. Several publications document the design process for shallow (large radiating area, low max excursion), and long-throw (smaller radiating area, high max excursion) transducers [6, 11, 12].

If $F(x_{vc})$ is monotonously and smoothly increasing with x_{vc}, the spider is considered weakly nonlinear and it will result in harmonic distortion. If $F(x_{vc})$ is discontinuous or non-monotonous then the spider is considered strongly nonlinear. The effects of such a spider design can be observed in jumps of the transducer's resonant frequency with increasing drive level [13], or in buckling of one or more spider rolls at large excursions, resulting in a rapid jump of the voice coil excursion [5]. These effects can be very detrimental to the reproduced audio signal, and they can also pose real challenges for the FEM solver.

FEM solvers solve a system of equations that relies on an equilibrium of forces and moments. When solving non-linear problems, the solvers iteratively solve for this equilibrium and discontinuous force-displacement relationships can severly impede solver convergence. Sometimes the solvers cannot find any solution that fulfills the equilibrium and return an error message instead. This becomes particularly problematic when FEM solvers are used in conjunction with numerical optimization algorithms, as these algorithms rely on evaluating FEM models with many different design parameter combinations. If the FEM solver cannot converge for one particular combination of parameters, the optimization algorithm will abort too. The solvers thus need to be robust against failure due to non-convergence.

First, we describe a simple method to augment conventional FEM solvers with an equation to improve their robustness in convergence when encountering buckling. We then show three parametric studies where we attempt to find a maximally linear spider with large excursion capabilities. The power of the augmented method is finally demonstrated in an optimization problem, where it is paramount that the FEM solver can solve for the force-deflection curve for all excursion values, even beyond buckling events.

2 Spider Buckling

Bolaños [5] describes how compression stresses can cause a spider roll to buckle. In generalized terms, buckling occurs when a loaded structure has a lower total potential energy V in the buckled configuration than it does in the unbuckled configuration. The potential energy V can be written as a function of strain energy U_{strain} and work performed by external forces W.

$$V = U_{strain} - W, \tag{1}$$

where W can generally be defined as the sum of the dot products of the externally applied forces $\vec{P}_i$ and the displacements $\vec{u}_i$ at the locations of the applied forces.

$$W = \sum_i \vec{P}_i \cdot \vec{u}_i \tag{2}$$

and U_{strain} can be calculated by integrating the product of stresses σ and strains ε over the entire structure domain Ω.

$$U_{strain} = \frac{1}{2} \oint \sigma \varepsilon d\Omega \tag{3}$$

Closed-form solutions for critical loads P_i or displacements u_i can be found in statics textbooks for some simple geometries like slender columns, beams, or rectangular plates. But for a general geometry like a spider it not possible to define a closed-form solution to determine the critical loads $\vec{P}_i$ or displacements $\vec{u}_i$ of an unstable configuration that leads to buckling. In such cases, the nonlinear force-deflection curve $F(x_{vc})$ can be calculated to infer buckling behavior.

A typical calculation of the force-deflection curve can be done in two analogous ways: impose a prescribed

voice coil displacement x_{vc} at the inner radius of the spider and calculate the restoring force $F(x_{vc})$ by finding the static equilibrium state, and then repeat the calculation for $-x_{max} \leq x_{vc} \leq x_{max}$, where x_{max} is the maximal allowable voice-coil excursion.

Alternatively, one can prescribe a force F at the inner radius of the spider and calculate the resulting displacement $x_{vc}(F)$. Plotting F vs $x_{vc}(F)$ then yields the desired force-displacement curve. This latter method is generally favored in FEM simulations, since a finite physical force will always results in a finite physical displacement. With the former method, it is conceivable to request a deformation that is incompatible with the degrees of freedom in the structure, which would be an ill-posed problem to solve.

If the method of prescribing F and solving for $x_{vc}(F)$ is used, one needs to know the necessary forces F_{min} and F_{max} to displace the voice-coil from $-x_{max}$ to x_{max}. The designer might be tempted to define the range of F_{min} to F_{max} with a large enough margin to overshoot the mechanical limits of the voice-coil excursion. This leads to unnecessary calculations and does not suit itself for a numerical optimization where the relationship between F and x_{vc} is only of interest within the mechanical limits of $\pm x_{max}$.

In order to solve the conundrum presented above, we propose an augmented FEM method that solves an additional algebraic equation in combination with the system of equations for the FEM solution. This is very similar to using a Riks solver [14], but it can be implemented for quasi-static problems in most FEM software packages by adding the following equation to the system of FEM equations:

$$x - \hat{x} = 0 \tag{4}$$

where $\hat{x}_{vc}$ is the "desired" voice-coil excursion for the yet-unknown applied force F. Solving the FEM equations with addition of (4), one essentially solves for the static equilibrium with prescribed force, without knowing F_{min}, F_{max} to result in a voice-coil displacement equivalent to $\pm\hat{x}$.

2.1 Simple Beam Buckling

To illustrate the above method, we first apply it to a simple steel beam that is loaded on-axis. The beam has length L = 3 m, a square cross-sectional shape of width d = 0.1 m, and is made of steel with Young's modulus E = 210 GPa. Any statics textbook will define the critical axial buckling load P_{cr} for a slender beam in a pinned-slider configuration as

$$P_{cr} = \frac{\pi^2 EI}{L^2}. \tag{5}$$

For the above beam dimension and an moment of area for a square cross-section $I = d^4/12$, we can calculate the critical buckling force to be $P_{cr} = 1.9 \times 10^6$ N. A "perfectly straight" numerical FEM model does not exhibit buckling, unless a small eccentricity is applied to either the force or the geometry. To test this case we applied an initial slight eccentricity of Δy = 0.1 mm at the center of the beam. Figure 2 shows a diagram of the simple beam in its initial and buckled configuration. Figure 3 shows the simulated force-deflection curve of the buckling beam compared to a perfect beam as well as the deflection Δy of the beam center-point.

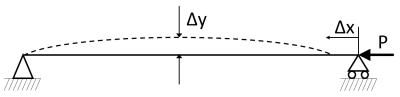

Fig. 2: Diagram of a simply supported beam with axial load in its initial (solid) and buckled (dashed) state.

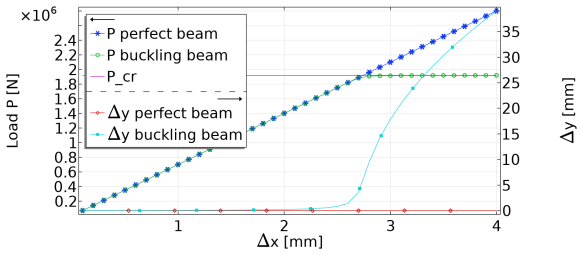

Fig. 3: Force-Deflection simulation for a simple beam with and without a small eccentricity at its center. Δy is the lateral deflection for the beam's center-point.

As can be seen, the simulation with the augmented FEM method perfectly captures the analytical critical load P_{crit} and it can be used to predict the behavior after initial buckling. The nearly horizontal force-deflection curve after the beam has buckled indicates that stiffness of the simple beam has reduced from about 0.7×10^6 N/mm to only 4.3×10^3 N/mm. This test case serves as validation example that the aug-

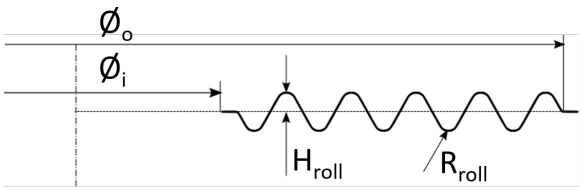

Fig. 4: Design parameters used in this study are the roll height H_{roll}, and roll radius R_{roll}. The other paramers are assumed to be fixed, including the inner diameter $\varnothing_i$, and outer diameter $\varnothing_o$.

mented FEM method presented here works to simulate buckling and post-buckling behavior.

2.2 Spider Design For Large-Excursion Woofer

A loudspeaker engineering study is presented for a spider used in a woofer with a 50.8-mm (2-inch) voice-coil with high-excursion capabilities. The mechanical excursion limit was required to be at least 30 mm. Tight space constraints in the enclosure allowed for a maximal outer spider diameter of only 152.4 mm (6 inches).

Under these space constraints we would like to design a spider with maximally linear force-deflection behavior all the way to the maximal voice-coil excursion limit of $x_{max} = 30$ mm. To keep the number of variables to a manageable limit in this paper, we will only consider spider geometries comprising of straight sections coupled to tangential circular arcs at the tips of the spider $N_{roll} = 10$ rolls, and spider material thickness of 0.5 mm. The material parameters are also kept constant with a Young's modulus of $E = 500$ MPa, density of $\rho = 600$ kg/m^3, and a Poisson's ratio of $\nu = 0.33$. The basic spider geometry and remaining parameters H_{roll} and R_{roll} are shown in Figure 4.

2.2.1 Spider Roll Height Study

As a first study, we vary the overall spider half-roll height from 1.5 mm to 6 mm. The radius of the roll tips is kept constant at 1.5 mm (measured at center line of spider material thickness). As can be seen in Figure 5, the shallower rolls result in spiders that are relatively soft (flat tangent) near the rest position of $x_{vc} = 0$ and become increasingly stiff (steep tangent) at higher excursion. This behavior is explained by the fact that the rolls get stretched completely. A spider with roll heights of 1.5 mm does not allow for

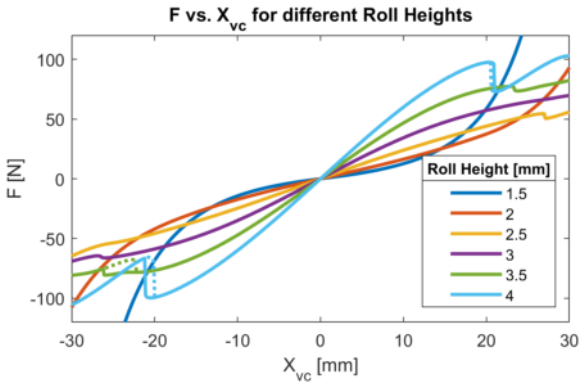

Fig. 5: Effect of roll height on force-deflection curve. At rest position, shallow rolls are softer than tall rolls. At large excursion, shallow rolls are stiffer than tall rolls. Solid line is out-stroke, and dotted line is back-stroke.

a full voice coil excursion to ± 30 mm. In contrast, spiders with tall rolls are stiffer near the rest position and become increasingly soft at higher excursions, up to a point where buckling occurs (jog in curve). The excursion at which buckling occurs can also depend on whether the spider is undergoing an out-stroke (increasing $|x_{vc}|$) or a back-stroke (decreasing $|x_{vc}|$). This can be seen for example in the curve of the spider with $H_{roll} = 3.5$ mm, where buckling on the negative out-stroke happens around $x_{vc} = -27$ mm (solid green curve), but on the back-stroke the buckled state is maintained until about $x_{vc} = 22$ mm (dotted green curve) before the spider reverts back to the unbuckled state. This asymmetric behavior results from the fact that the buckled state is at lower potential energy V than the unbuckled state. For the buckling to reverse itself, the excursion must thus be reduced beyond the initial buckling point.

With regards to the aim of achieving maximally linear spider, the spider with roll height of 2.5 mm is the best candidate in this first round. However, the force-deflection curve for this spider indicates that it buckles at $x_{vc} = 27$ mm.

Figure 6 shows the spider deformation for a number of voice coil positions of the spider with a roll height of 4 mm. For spider excursions between 0 mm and 20 mm, the deformation is fairly uniform between the rolls, but at 25 mm and 30 mm the outermost roll is clearly over-stretched, indicating that buckling had occurred. From

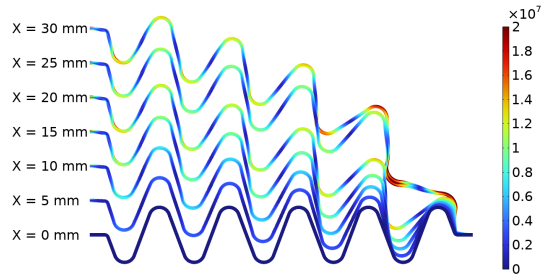

Fig. 6: Deformation of spider with H_{roll} of 4 mm at different voice coil excursions during the out-stroke. Buckling occurs between $x_{vc} = 20$ mm and $x_{vc} = 25$ mm. Color indicates the von Mises stress in the spider material in units of Pa.

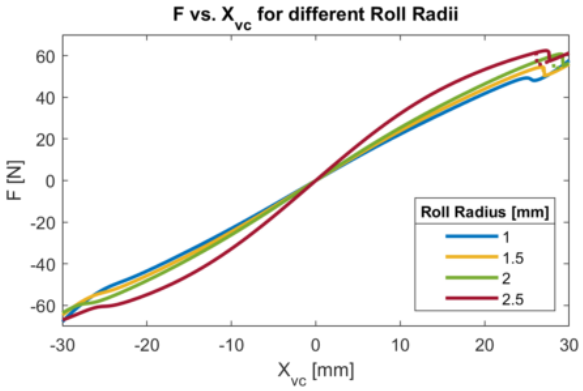

Fig. 7: Force-deflection curve for spiders with different roll radii. Solid lines are for the out-stroke and dotted lines are for the back-stroke.

Figure 5, one can see that the buckling occurs at a voice coil excursion between 21 and 22 mm.

2.2.2 Spider Roll Radius Study

In a second study, we investigate the effect of the roll radius, while keeping the roll height and other parameters constant. Figure 7 shows the force-deflection curves for spiders with roll height of $R_{roll} = 2.5$ mm and roll radii R_{roll} between 1 mm and 2.5 mm. The figure shows that all four versions show buckling behavior at high positive excursion. The largest roll radius shows the most non-linear behavior and the other examples are relatively linear up to ± 24 mm excursion.

However, when looking at the maximal von Mises stress in the spider (see Figure 8), one can see that the

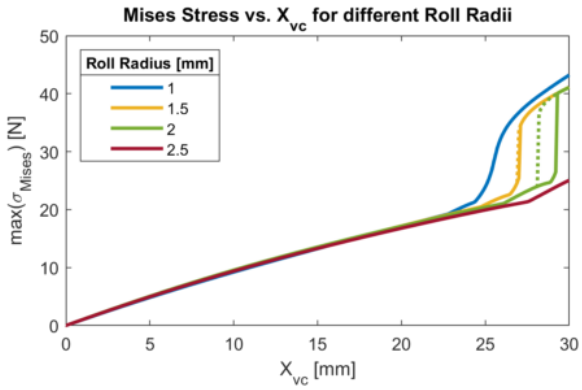

Fig. 8: Maximal von Mises stresses in spiders with different roll radii during the positive excursion. Solid lines are for the out-stroke and dotted lines are for the back-stroke.

small roll radii yield stresses that are about 2x higher, which could cause cracking in the spider matrix material. None of the simulated spiders satisfy the requirement of avoiding buckling and linear force-deflection curve for excursions in the range of ± 30 mm. Even small buckling bumps in the force-deflection curve can yield audible and unwanted distortion. Thus the search for a suitable spider geometry must continue.

2.2.3 Progressive and Regressive Spider Roll Height

Observation of plots like the one shown in Figure 6 suggest that the stress distribution in the spider rolls is not uniform. Typically the rolls near the outer edge of the spider show significantly larger stresses than the remaining rolls. This suggests that a uniform roll shape with equal height and roll radius might not be the optimal solution for a large-excursion spider. Hutt claimed that a "regressive" spider geometry with roll heights that diminish with increasing radius is optimal in terms of linearity and frequency shift with increasing power [1]. We have thus run a study of spider geometries with varying roll height. The mean half-roll height is kept constant at $H^* = 2.5$ mm, and the change in roll height is defined to be linear. The difference between outermost and innermost half-roll height is defined as ΔH, and the height of the individual half-rolls H_j is given as

$$H_j = H^* - \frac{\Delta H}{2} + (j-1)\frac{\Delta H}{N_{roll}-1}, j \in (1, N_{roll}) \quad (6)$$

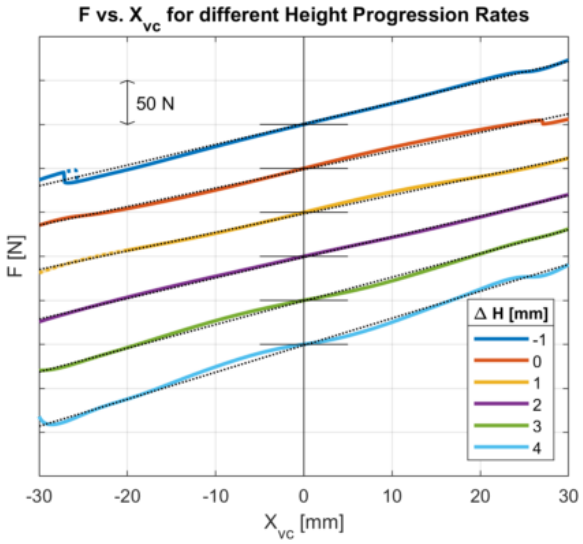

Fig. 9: Force-Deflection curves for progressive and regressive spiders. Each curve is offset by 50 N to better show the differences. The thin dotted black lines show the linear regression for each case. Solid colored lines are for the outstroke, and dashed colored lines are for the back-stroke.

With this formula and positive value for ΔH, the innermost half-roll height H_1 is ΔH shorter than the outermost half-roll height $H_{N_{roll}}$, and the average half-roll height is H^*. This is considered a "progressive roll height" spider. When ΔH is negative, the innermost half-roll is taller than the outermost half-roll and is considered a "regressive roll height" spider. The resulting force-deflection curves for the progressive and regressive spider designs are shown in Figure 9.

This result shows that it is possible to design a spider geometry with the given constraints that will not buckle within the excursion range of ± 30 mm. Progressive spiders with mean half-roll height of $H^* = 2.5$ mm and ΔH between 1 mm and 3 mm do not show signs of buckling. Furthermore, the example with $\Delta H = 2$ mm shows a very linear force-deflection curve. Further improvement might be achieved by varying the roll radii as well, but that has not been studied for this work.

2.2.4 Roll Height Optimization

The great advantage of being able to simulate $F(x_{VC})$ past the point buckling is the ability to employ numerical optimization routines to a problem without getting bogged down by solver problems. Numerical optimization methods require the objective function to be relatively smooth across the design space. If a solver cannot finish an evaluation due to singularities like a buckling event, then the optimizer cannot know what value to apply. Simply applying an artificially large objective value can lead to optimized non-convergence or drive the search for an optimal set of parameters far away from the true optimal solution. To demonstrate that the presented augmented buckling simulation method indeed can be applied to spider design, we have let the optimizer find an optimal set of half-roll heights H_j, with the objective to linearize the force-deflection curve as much as possible.

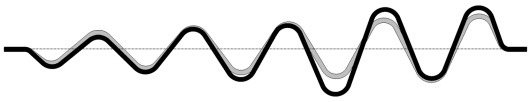

Fig. 10: Optimized spider geometry (black) and initial guess (gray). H_j progression is not monotonous anymore, but the geometry does improve the symmetry of the force-deflection curve.

The best design from the previous study ($H^* = 2.5$ mm, $\Delta H = 2$ mm, $R_{roll} = 1.5$ mm) is taken as initial design and the optimizer is allowed to vary the individual half-roll heights H_j between 0.5 mm and 6 mm. We employ a parametric strategy [7], and a gradient-free Nelder-Mead optimization solver [15], along with a least-squares objective between the force-deflection curve and its linear regression as objective function. The initial guess and resulting optimized geometry can be seen in Figure 10, and the optimized individual half-roll heights are listed in Table 1.

The least squares error between the force deflection curve and its linear regression is reduced from 0.0853 N for the initial guess to 0.0116 N for the optimized solution. If the linearized force deflection curves were to be calculated to a spider stiffness value, then the designs result in $K_{ms} = 0.583$ N/mm for the initial guess, and an almost identical $K_{ms} = 0.584$ N/mm for the optimized solution.

Table 1: The values of the optimized half-roll heights H_j.

j	1	2	3	4	5	6	7	8	9	10
H_j [mm]	1.85	1.30	2.41	2.22	3.15	2.54	4.79	4.24	3.11	4.43

3 Conclusion

We have demonstrated an augmented FEM method that allows the simulation of force-deflection curves for loudspeaker spiders past buckling events that can occur at large excursion. Without such an augmented method, the standard FEM solvers will not converge to a solution at the point of buckling. We have presented three parametric studies to illustrate how spider design can be pushed to the extreme by optimizing a spider that can operate nearly linear for large excursions of ± 30 mm, despite its constraining dimensions. The augmented method presented is even robust enough to be used in a numerical optimization where some of the intermediate solutions will result in buckling. Without this robust solution method, numerical optimization would not be possible.

We point out the fact that we have used an isotropic material, but real-world spiders are typically made of an impregnated fabric. Such materials are better described by material models that have different properties in different directions. With the isotropic material assumption, it was also possible to use axi-symmetric FEM models to more quickly iterate between different designs.

4 Acknowledgements

Samsung Electronics and Samsung Research America supported this work. The authors would like to thank the entire staff of Samsung's US Audio Lab who helped with all aspects of this research, offered insightful suggestions, and contributed to this work.

References

[1] Hutt, S., "Loudspeaker Spider Linearity," *Audio Engineering Society Convention 108*, p. 5159, 2000.

[2] Brunet, P. and Kubota, G., "Nonlinear Control of Loudspeaker Based On Output Flatness and Trajectory Planning," *Audio Engineering Society 147*, p. 10241, 2019.

[3] Brunet, P., Li, Y., Kubota, G., and Mariajohn, A., "Application of AI Techniques for Nonlinear Control of Loudspeakers," *Audio Engineering Society Convention 151*, p. 10535, 2021.

[4] Rausch, M., Kaltenbacher, M., Landes, H., Lerch, R., Kreitmeier, L., and Krump, G., "Computer-Aided Design of Electrodynamic Loudspeakers by Using a Finite Element Method," *Audio Engineering Society Convention 111*, p. 5420, 2001.

[5] Bolaños, F., "Stress Analysis on Moving Assemblies and Suspensions of Loudspeakers," *Audio Engineering Society - 121st Convention Papers 2006*, 2, pp. 928–947, 2006.

[6] Martinez, J., Segovie, E., Ramis, J., Espi, A., and Carbajo, J., "An approach to small size direct radiation transducers with high SPL," *Audio Engineering Society 131*, p. 8467, 2011.

[7] Bezzola, A., "Numerical Optimization Strategies for Acoustic Elements in Loudspeaker Design," in *Audio Engineering Society Convention 145*, New York City, 2018.

[8] COMSOL AB, "Loudspeaker Spider Optimization," 2022.

[9] Christensen, R., "Shape and Topology Optimization of Loudspeaker Drivers," *Comsol Conference Europe*, 2020.

[10] Nielsen, D. G., "Achieving a flat, wideband frequency response of a loudspeaker unit by numerical optimization with requirements on its directivity," *The Journal of the Acoustical Society of America*, 150(2), p. 663, 2021, doi: 0.1121/10.0005731.

[11] Futtrup, C., "Design Considerations for Shallow Subwoofers," *Audio Engineering Society Convention 121*, 2, p. 6944, 2006.

[12] Button, D. J., "Design Parameters and Trade-Offs in Large Diameter Transducers," *Audio Engineering Society Convention 91*, p. 3192, 1991.

[13] Jabbari, A. and Unruh, A., "Jump Resonance in Audio Transducers," *Audio Engineering Society Convention 117*, p. 6247, 2004.

[14] Riks, E., "An incremental approach to the solution of snapping and buckling problems," *International Journal of Solids and Structures*, 15(7), pp. 529–551, 1979, ISSN 00207683, doi: 10.1016/0020-7683(79)90081-7.

[15] Conn, A. R., Scheinberg, K., and Vicente, L. N., *Introduction to Derivative-Free Optimization*, SIAM, 2009, ISBN 978-0-898716-68-9.